MICRO-MECHANICAL DAMAGE MODELLING OF NOTCHED BAR TESTING OF MODERN LINE PIPE STEEL

S. H. Hashemi, I. C. Howard, J. R. Yates and R. M. Andrews*
The University of Sheffield, Department of Mechanical Engineering, Sheffield, UK
*Advantica Technologies Ltd, Loughborough, UK
s.h.hashemi@shef.ac.uk

Summary

This paper reports work on the modelling of flat fracture in modern gas pipeline steels. Experimental data from typical tensile bars together with damage mechanics theories has been used to capture flat fracture characteristics of gas pipeline steel of grade API X100. This is required for subsequent analysis of Charpy impact specimen to isolate that part of the absorbed energy associated with flat fracture appearance on the centre of the Charpy fracture surface.

The results of this study showed that typical damage parameters of the modified Gurson model for ductile fracture are applicable to high-grade X100 steel. The numerical analysis was able to simulate the necking of all tensile specimens. However, a small value of void volume fraction was required to trigger the damage in the centre of FE model where the stress triaxiality was high. The final stage of crack propagation in test samples was dominated by slant fracture. An average stress triaxiality of 0.88 was able to characterise the onset of the flat-to-slant fracture transition in all tensile specimens. The specific flat fracture energy was 1.0 J/mm^2 for this steel.

Introduction

A major concern for the designers and operators of high-pressure gas transmission pipelines made from high-strength steels is the control of long running ductile fractures. Current practice is to control fracture propagation by specifying an upper shelf Charpy energy using various semi-empirical models. Full-scale fracture propagation tests on modern high-strength steels, for example Demofonti et al. [1], have shown that these models become increasingly inaccurate as the steel strength increases. It has been revealed that propagation/arrest prediction models based on total Charpy absorbed fracture energy require extremely high levels of material fracture toughness for X100 steel (of the order of 400J or above in terms of Charpy impact energy) which is physically impractical [2]. This has led to different amendments and use of various correction factors for a better correlation between the test and the prediction model [3]. However, the Charpy test data actually does contain information connected with the pipeline failure mechanisms. Typically the Charpy fracture surface on the upper shelf contains flat fracture at the centre and shear lips at the edges. Hence a potential way forward is to isolate the part of the Charpy energy that is associated with the slant shear fracture, discarding the flat fracture information and other effects such as overall plastic deformation. To do this, accurate models of the flat and slant fracture processes are required.

The research reported here describes recent results on the modelling of the flat fracture in high-strength pipeline steel of grade API X100. Details of the test and computational work on

slant fracture of the X100 steel are set out in reference [4]. In the current work, the experimental load-diametral contraction data from tensile bars was used together with damage mechanics theories to model the fracture characteristics of the test specimens. Although the material was anisotropic (due to the pipe rolling schedule), an isotropic axi-symmetric finite element model was able to simulate the mean load-diametral variation in the pipe thickness direction. Typical Gurson damage parameters for flat fracture proved to be applicable to high-strength low-alloy X100 steel. However a small critical void volume fraction of the order of 0.001 was needed to trigger the damage at the centre of the FE model where the restraint was high.

Material properties

The material under investigation was an API X100 grade gas pipe (36" O.D×19mm W.T). The measured mechanical properties of the material and its chemical composition are set out in Tables 1 and 2.

Table 1. X100 steel mechanical properties in transverse direction

Young's modulus GPa	Yield strength (0.2% proof stress) MPa	Tensile strength MPa	Yield/UTS
210	769	823	0.93

Table 2. X100 steel chemical composition reported by the pipe manufacturer

element	C	Si	Mn	P	S	Cu	Ni	Cr	Mo	Nb	Ti	Al
(wt%)	0.06	0.18	1.84	0.008	0.001	0.31	0.5	0.03	0.25	0.05	0.018	0.036

The true stress-strain data required for FEA was obtained from the tensile tests on plain bar specimens, see Fig. 1.

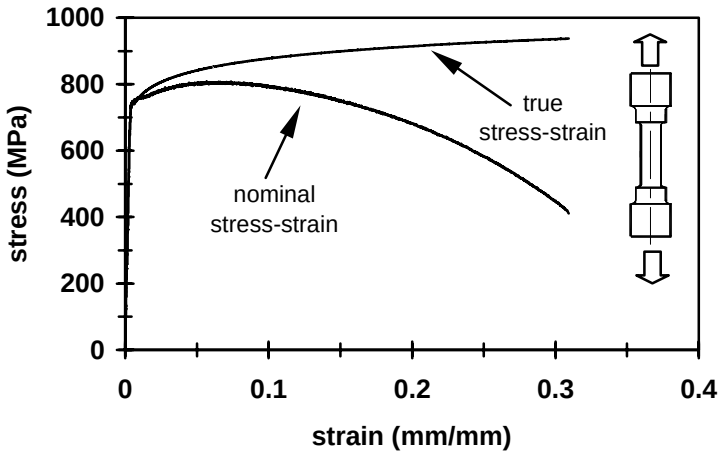

FIGURE 1. Nominal and true stress-strain curves for X100 steel

Experimental work

Smooth and notched round tensile bars were taken from the original pipe in the transverse orientation and tested on a servo-hydraulic Instron 8501 test machine with hydraulic grips under displacement control of 0.01mm/s. A transverse extensometer was used to capture the reduction of specimen diameter in each test. This was subsequently used for tuning the finite element damage model for flat fracture.

Three sets of laboratory specimens with different gauge diameter and notch acuity (i.e. different constraint levels at the gauge section of the test specimen) provided sufficient data to study the ductile flat fracture characteristics of X100 steel. The design dimensions of the tensile specimens are given in Table 3.

Table 3. Specifications of notched tensile specimens

tensile specimens	number of specimens	gauge length (mm)	gauge diameter (mm)	notch curvature ρ (mm)	notch diameter $2R_o$ (mm)	$\frac{R_o}{\rho}$
smooth	3	40	10	∞	10	0
notched –1st set	3	40	10	5.8	8	0.7
notched –2nd set	3	40	10	2	6	1.5

Due to the rolling schedule of the pipe, the material was highly anisotropic. All tensile specimens suffered considerable ovalisation. Fig. 2 illustrates the deformed cross section of a plain tensile specimen with the minor and major axes in the pipe thickness and axial orientations, respectively.

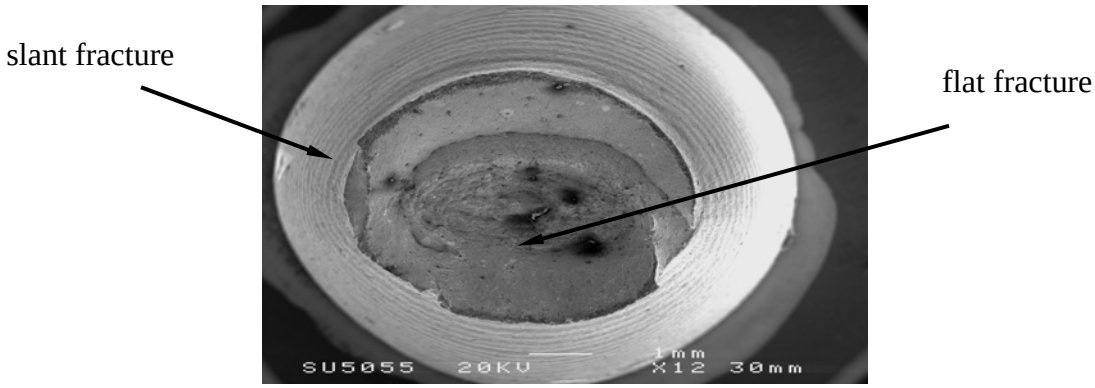

FIGURE 2. SEM of oval cross section from plain bar tensile specimen

The directional properties of the X100 steel led to different load-diametral contraction in the pipe thickness and axial directions as shown in Fig. 3.

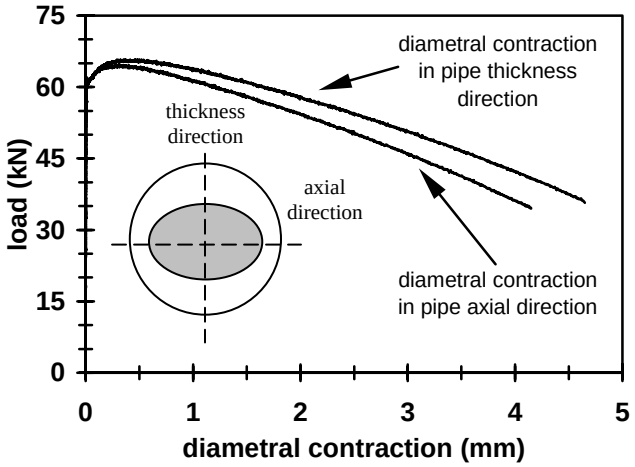

FIGURE 3. Load-diametral contraction for plain par tensile specimen

Finite element analysis

The simulation of all test specimens was carried out using the modified Gurson ductile damage theory [5,6] and the commercial finite element code ABAQUS 6.2 [7]. The Gurson yield potential is typically expressed as:

$$\Phi = (\frac{\sigma_{eq}}{\sigma_Y})^2 + 2q_1 f \cosh(-q_2 \frac{3p}{2\sigma_Y}) - (1 + q_3 f^{\,2}) = 0 \qquad (1)$$

where σ_{eq} is the von Mises equivalent stress, σ_Y the material yield strength, p the hydrostatic pressure, q_1, q_2 and q_3 are material constants, and f is the damage parameter. The values of the q parameters are typically around $q_1 = 1.5$, $q_2 = 1.0$ and $q_3 = q_1^2$ for ferritic steels.

In this model, fracture propagates when the damage parameter reaches its critical value designated by f_c (threshold of rapid loss of stress carrying capacity). The damaged elements are removed from the analysis simulating crack growth through the microstructure. The final void volume fraction at total failure is represented by f_f. These two, as well as q_1 and q_2, are considered as material constants. Therefore, in total, four constants should be determined to perform the damage simulation.

The initial void volume fraction of X100 steel can be calculated from Franklin's formula [8]:

$$f_o = f_v \frac{(d_x d_y)^{\frac{1}{2}}}{d_z} \qquad (2)$$

$$f_v = 0.054(S\% - \frac{0.001}{Mn\%}) \qquad (3)$$

where d_x, d_y and d_z are the average dimensions of the inclusions. If a spherical inclusion shape is assumed, equation (2) gives $f_o = f_v$. From this an initial void volume fraction $f_0 = 3\times10^{-5}$ was found for this steel.

Typical values of the q parameters were used to start the simulation. The critical and final void volume fraction was determined by a trial and error procedure until the model response matched the experimental data.

Another important parameter in the model is the critical mesh size l_c which is a representative of the average inter-particle distance. It is a representative of the average inter-particle distance and is determined either by SEM study or from the FE analysis. In this research the latter was used to find the proper cell size. A value of l_c = 200μm was found to work well for all tested specimens. This was transferable to different numerical models.

FE analysis showed that the damage theory was able to simulate the failure behaviour of all test samples. Typical Gurson damage parameters for flat fracture proved to be applicable to this high-strength low-alloy X100 steel. The values of the calibrated damage parameters are listed in Table 4. A small critical void volume fraction $f_c = 0.001$ (compared with a typical value of 0.15) was needed to trigger the damage at the centre of the FE model.

Table 4. Damage modelling parameters used in FE analysis of flat fracture

q_1	q_2	q_3	l_c (mm)	f_o	f_c	f_f
1.5	1.05	2.25	0.2	3×10^{-5}	0.001	0.005

Results and discussion

Fig. 4 shows the contour plots of void volume fraction in a smooth tensile specimen before the damage of the central elements. Due to high levels of stress triaxiality, the maximum cavity occurs in the centre of the specimen resulting in high values of void volume fraction. When the void volume fraction reaches its critical value, the central elements are failed and removed from the analysis. The failure of subsequent elements occurs in the same manner simulating the progression of flat fracture in the horizontal symmetry plane of the model.

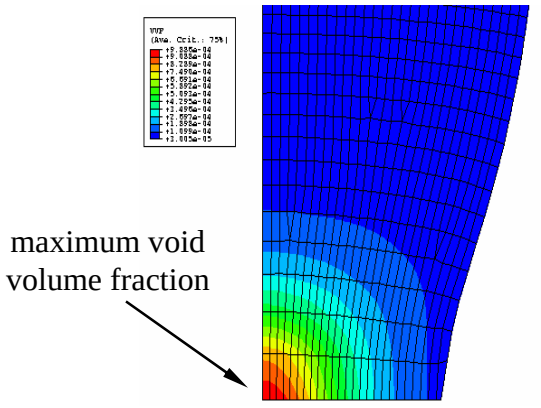

FIGURE 4. Contour plots of void volume fraction in plain bar tensile model before the failure of the central elements

Fig. 5 is the results of the test and simulation on different tensile specimens.

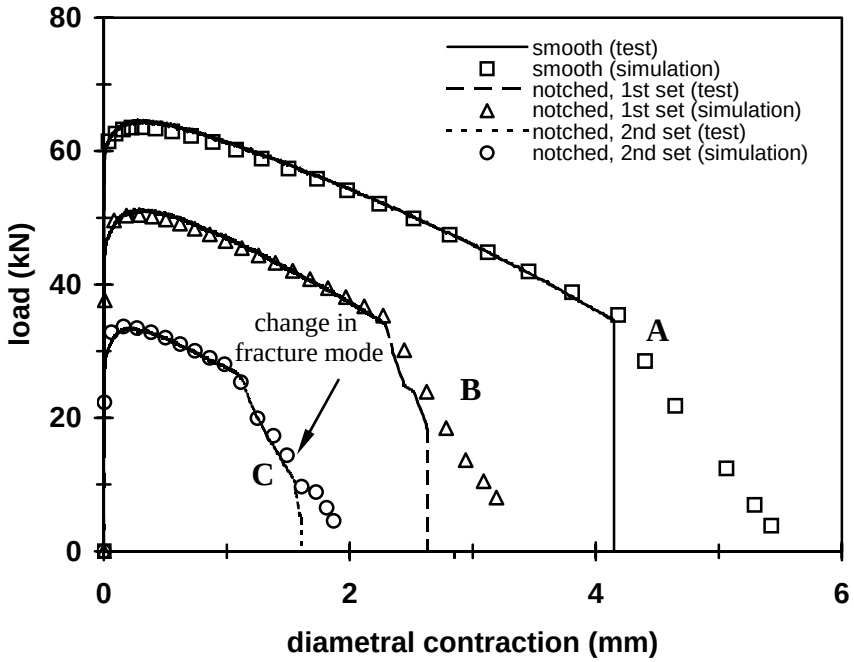

FIGURE 5. Load-diametral contraction from smooth and notched tensile bars

The comparison of the results of tests and numerical simulations shows good agreement in the softening region except at the tail part of the plots. This shows that the micro-mechanical damage models calibrated on flat fracture are transferable from one set of test specimen to others with different restraints and geometry. The disagreement between the tests and FE models (starting from points A, B and C in the load-diametral contraction diagrams) is a result of the fracture mode transition from flat to slant, see Fig. 6. The final stage of crack propagation in tensile specimens is dominated by slant fracture. Therefore, a different model is required to represent this failure mechanism.

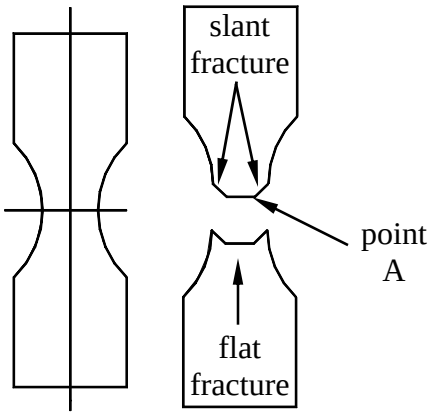

FIGURE 6. Schematic of necking of smooth tensile bar (left) and cup-cone formation(right) (point A is associated with the sudden load drop shown in plots of load-diametral contraction)

Fig. 6 shows the necking of a smooth tensile specimen and the subsequent shear fracture propagation near its surface. The flat fracture in the centre of the specimen is associated with a plane strain stress state. Near the free surface of the specimen, the stress conditions are plane stress. This causes shear band formation at the edges of the specimen resulting in a flat to slant fracture transition. Consequently, a crack having either +45 or -45 degree (depending on which quarter of the specimen is being modelled) is formed and propagates towards the specimen surface. The result is the cup and cone formation on the fracture surface of the broken specimen (see Fig. 2).

Fig. 7 is the distribution of shear stresses in the smooth tensile specimen shortly before and after the failure of the central elements. The localisation of shear stresses at the edges of the specimen and the orientation of shear fracture propagation can be observed in this diagram.

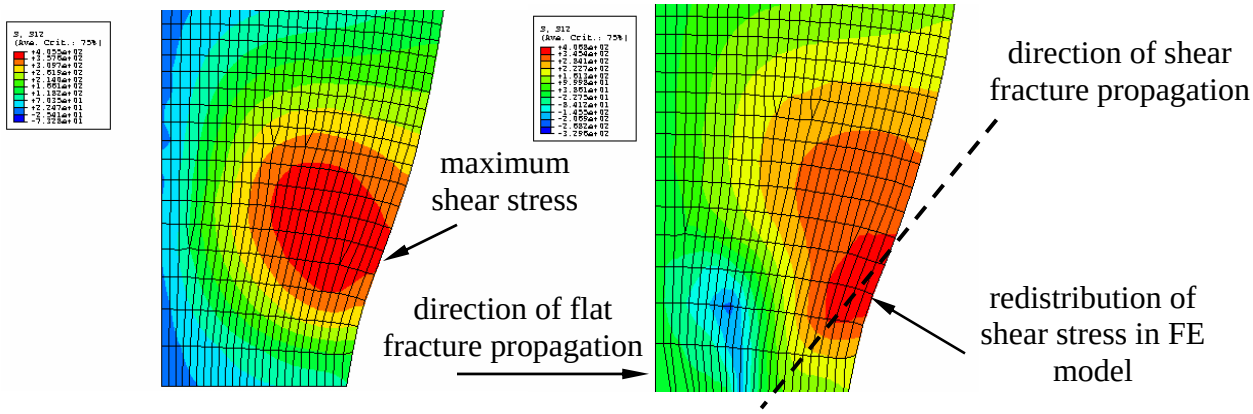

FIGURE 7. Contour plots of shear stresses in plain bar tensile model before (left) and their redistribution after the failure of central elements (right)

The information on this flat-to-slant fracture transition derived from the FEA is given in Table 5.

Table 5. Flat-to-slant fracture transition data from FE models

specimen	point	load P (kN)	P/P_{max}	diameter d (mm)	$d/2R_o$	Δa mm	flat fracture energy (J/mm^2)	shear stress (MPa)	$\frac{\sigma_m}{\sigma_{eq}}$
smooth bar	A	28.5	44%	5.6	56%	1.65	1.3	404	0.90
notched - 1st set	B	18.5	36%	5.2	65%	2.25	1.0	403	0.86
notched - 2nd set	C	9.7	29%	4.4	73%	2.31	0.8	402	0.87

Fig. 8 shows the stress triaxiality data ($\tau = \sigma_m / \sigma_{eq}$, where σ_m is the mean stress and σ_{eq} the von Mises equivalent stress) in different sets of tensile bars at the onset of flat fracture in the centre of the models and the onset of slant fracture near their surfaces. As can be seen, stress triaxiality is a linear progressing function of the ratio of notch radius to notch curvature (R_o / ρ). At the onset of flat fracture, the stress triaxiality was maximum in the second sets of notched specimens with a sharp notch. At the onset of slant fracture, stress triaxiality ahead of the crack tip in both sets of notched specimens had similar values. These were consistent with stress

triaxiality values of the smooth specimens. Interestingly, shear stresses ahead of the crack tip were similar in all tensile bars. This suggests that in tensile testing of this X100 steel, the transition from flat to slant fracture can be characterised by an average stress triaxiality value of the order of 0.88.

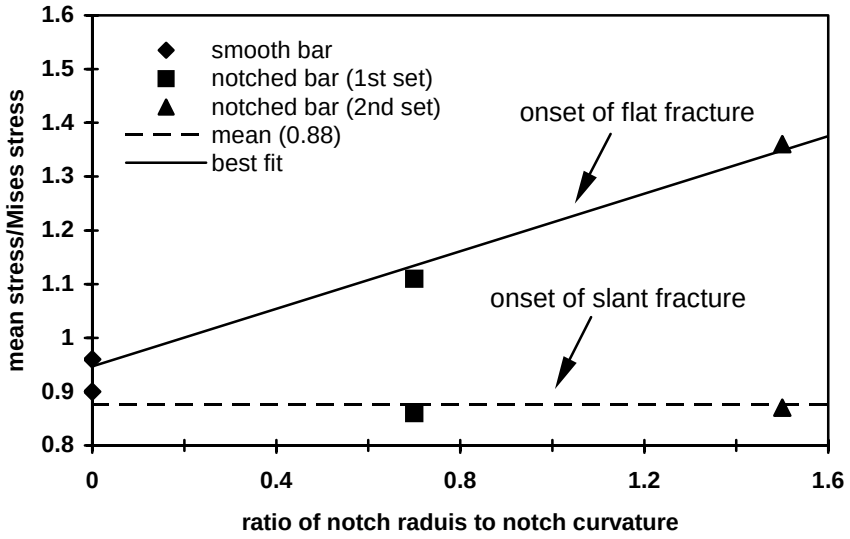

FIGURE 8. Comparison of stress triaxiality values in different sets of tensile specimens

Fracture information presented in Table 5 gives an average value 1.0 (J/mm^2) for the energy consumption rate during the flat fracture propagation in this steel. This agrees well with the value of 1.1 (J/mm^2) for the flat fracture specific energy in the same material measured on standard C(T) specimens [4], and with similar data reported by Stampfl and Kolednik [9].

Conclusion

The experimental data from tensile bars used together with the damage mechanics theories was able to simulate the observed behaviour of tensile specimens made from high-toughness pipeline steel of grade X100. An isotropic axi-symmetric model was able to simulate the mean load-diametral variation in the pipe thickness direction. Typical Gurson damage parameters for flat fracture proved to be applicable to high-strength low-alloy X100 steel. However, a small critical void volume fraction $f_c = 0.001$ was needed to trigger the damage at the centre of the FE model where the stress triaxiality was high. An average value 0.88 of stress triaxiality was able to characterise the onset of the flat-to-slant fracture transition in all tensile bars.

References

1. Demofonti, G., Mannucci, G., Spinelli, C. M., Barsanti, L. and Hillenbrand, H. G., In *Proceedings of Pipeline Technology*, edited by R. Denys, Elsevier Science, 2000, 509-520.

2. Makino, H., Kubo, T., Shiwaku, T., Endo, S., Inoue, T., Kawaguchi, Y., Matsumoto, Y. and Machida, S., *ISIJ International*, Vol. **41**, No. 4, 2001, 381-388.
3. Leis, B. N., Eiber, R. J., Carlson, L. and Gilroy-Scott, A., In *Proceedings of International Pipeline Conference*, Vol. **II**, ASME, 1998, 723-731.
4. Hashemi, S. H., Howard, I. C., and Yates, J. R., *Submitted to ECF-15 for publication*, 2004.
5. Gurson, A. L., *Journal of Engineering Materials and Technology*, Vol. **99**, 1977, 2-15.
6. Tvergaard, V., *International Journal of Fracture Mechanics*, Vol. **17**, 1981, 389-407.
7. Hibbitt, H. D., Karlsson, B. I. and Sorensen, E. P., ABAQUS User's Manual (R. 6.2), 2001.
8. Franklin, A. G., *J. Iron and Steel Inst.*, **207**, 1969, 181-186.
9. Stampfl, J. and Kolednik, O., *Int. J. Fract*., Vol. **101**, 2000, 321-345.